Powder Technology 475 (2026) 122313

Contents lists available at ScienceDirect

Powder Technology

journal homepage: www.journals.elsevier.com/powder-technology

Linking roller compaction and tableting: Simple extensions of Kawakita and Ryshkewitch-Duckworth

Christian Eichler [a,b,*], Stefan Heinrich [a]

[a] Institute of Solid Process Engineering and Particle Technology, Hamburg University of Technology, Denickestrasse 15, 21073 Hamburg, Germany
[b] DyssolTEC GmbH, Harburger Schlossstraße 6-12, 21079 Hamburg, Germany

HIGHLIGHTS

- Unified model links roller compaction and tableting
- Prediction of tablet porosity and strength
- Reduced-order linkage of roller compaction and tableting using two lumped interface parameters

GRAPHICAL ABSTRACT

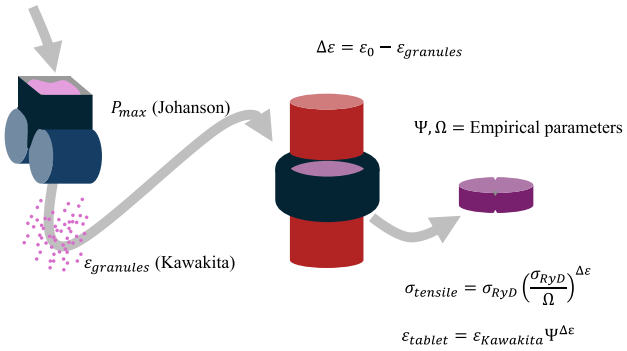

ARTICLE INFO

Keywords:
Roller compaction
Tablet press
Tableting
Johanson
Kawakita
Ryshkewitch-Duckworth
Global sensitivity analysis

ABSTRACT

Roller compaction (RC) is widely used in pharmaceutical manufacturing but produces ribbons with non-uniform porosity, complicating the prediction of tablet properties. Here, we present a reduced-order framework that links roller compaction and tableting by minimally extending established constitutive models to predict tablet porosity and tensile strength with low additional data demand. Peak RC stress was calculated using the Johanson model as a function of specific compaction force, while ribbon porosity was estimated with the Kawakita relation, which we extended to capture pre-compaction effects, enabling estimation of the final tablet porosity. Tablet tensile strength was described by the Ryshkewitch–Duckworth relation, extended by a pressure-like term representing granule hardening during pre-compaction.

A global sensitivity analysis was performed, and the framework was validated against literature data for microcrystalline cellulose (MCC) and mannitol, including response-surface evaluation over RC and tableting conditions. Fitting the empirical parameters yielded excellent agreement for tablet porosity (MCC: $R^2 = 0.99$; mannitol: $R^2 = 0.96$) and tensile strength when using experimental porosity (MCC: $R^2 = 0.98$; mannitol: $R^2 = 0.99$). Predicting tensile strength via model-predicted porosity remained strong. Sensitivity analysis identified tableting pressure and Kawakita model parameters as the dominant factors influencing final porosity and tensile strength.

* Corresponding author at: Institute of Solid Process Engineering and Particle Technology, Hamburg University of Technology, Denickestrasse 15, 21073 Hamburg, Germany.
E-mail addresses: christian.eichler@tuhh.de (C. Eichler), stefan.heinrich@tuhh.de (S. Heinrich).

https://doi.org/10.1016/j.powtec.2026.122313
Received 30 December 2025; Received in revised form 10 February 2026; Accepted 20 February 2026
Available online 21 February 2026

The two simple model extensions integrate RC and tableting into a unified, easy-to-apply framework suitable for parameter exploration and model-based design of experiments. Despite known simplifications, the framework consistently captured trends for both plastic and brittle excipients.

1. Introduction

The roller compaction (RC) process is widely used in pharmaceutical granulation, particularly for formulations containing moisture- or heat-sensitive materials. RC is a well-established technology that, by design, enables continuous manufacturing with relatively low energy consumption. The process consists of a compaction stage, in which ribbons are produced, and is typically followed by a milling stage to generate granules with the desired particle size distribution. Milling is most commonly performed using screen mills, which break the ribbons into the final dry granules.

The ribbons produced by roller compaction generally exhibit non-uniform porosity. Depending on the device configuration, either the ribbon center or its edges may show higher porosity [1–3]. When cheek plates are used, the stationary side sealing prevents powder from escaping the compaction zone but also shears the bulk material, leading to reduced mass at the ribbon edges and consequently higher porosity. In contrast, rimmed rollers provide a moving side seal that enhances material flow toward the edges, typically resulting in lower edge porosity. Additionally, the feeding system often consists of a screw feeder, which pushes material into the compaction zone and produces an oscillating track of elevated porosity across the ribbon [1,4–6]. As a result, ribbons – and consequently the granules derived from them – do not exhibit homogeneous porosity.

Modeling of the compaction process was already introduced by Johanson in 1965 [7]. His analytical approach assumed a nip angle, from which the bulk material moves at the same velocity as the rollers, and that the maximum compaction force occurs at the minimum gap. However, experimental measurements have demonstrated deviations from these assumptions [8–10]. Despite its limitations, the Johanson model remains widely used because it is straightforward to apply and provides an approximate estimate of peak compaction stress. Several extensions of the model have been proposed, including empirical adjustments to improve the accuracy of compaction pressure predictions [11–13] and approaches that incorporate a pressure distribution across the roller surface to better capture the ribbon porosity profile [14]. These modifications, however, introduce additional empirical parameters that require fitting.

In addition to analytical modeling, compaction simulations are commonly performed. Accordingly, tablets are compressed at a gradual compaction speed to mimic compaction between the rollers with the aim of predicting the ribbon porosity [15,16]. The specific compaction force (SCF) can be determined by integrating force over time [16]. Despite the gradual speed, porosity values from compaction simulation and RC differ and can be corrected via transfer learning [17].

In combination with the maximum compaction force, compressibility models such as those of Heckel [18,19], Kawakita [20,21], and Cooper–Eaton [22] are commonly applied to describe the relationship between compaction pressure and tablet porosity under uniaxial compression. After compaction, elastic recovery leads to expansion of the compacted body and increased porosity. The extent of this recovery depends on the material and the dwell time under load: longer dwell times generally reduce elastic recovery, particularly for plastically deforming materials [23–25]. Consequently, both in-die and out-of-die porosities can be described by these compressibility models.

During compression of dry-granulated granules, those formed in the roll compactor exhibit reduced porosity and increased mechanical strength compared to the original powder. This granule hardening effect makes them less deformable under subsequent tableting pressures, thereby reducing the bonding area available for interparticle interactions. Consequently, the tablet press must overcome the higher yield strength of these hardened granules to achieve additional bonding, leading to the commonly observed loss of tabletability after dry granulation [26]. As a result, tablets produced from RC granules show lower tensile strength than directly compacted tablets when compressed at the same force, although at lower porosity [27].

The reduction in tabletability has already been described within a modeling framework by Gavi et al. [28], who considered the process steps of RC, ribbon milling, and tableting to predict tablet tensile strength and dissolution. In their approach, the compressibility factor from the Johanson model (see Eq. (6)) was used to describe ribbon porosity, while tablet tensile strength was predicted using the model of Farber et al. [29]. The latter incorporates the pre-compaction porosity as an additional parameter, which brings challenges for RC ribbons because they exhibit a distribution of porosities rather than a single uniform value [29]. White et al. [30] further extended this framework by introducing an additional fitting parameter to improve predictive accuracy.

A less mechanistic and more automated approach was presented by Bachawala et al. [31], who applied normalized bivariate rational functions to link upstream process parameters to tablet properties. Their method achieved good agreement, but only for a single material and based on a large dataset (2400 tablets). Other studies have relied on extensive experimental data to derive models using multivariate analysis [32–34], which enables the identification of the most influential material parameters.

Although various modeling approaches have been proposed to link RC and tableting, their applicability remains limited when predicting the tabletability of new formulations with unknown material parameters. The present work therefore proposes a reduced-order framework for linking roller compaction and tableting, based on standard compaction and shear tests and supplemented by two lumped empirical parameters that capture pre-compaction effects.

2. Data and methods

2.1. Experimental data

This study uses solely data reported by Rajkumar et al. [27] for microcrystalline cellulose (MCC) and mannitol. Both are widely used excipients in the pharmaceutical industry; however, their mechanical properties differ substantially. MCC undergoes predominantly plastic deformation, whereas mannitol is brittle. These contrasting behaviors result in distinct tabletabilities and sensitivities to pre-compaction [27].

2.2. Johanson model

The Johanson model [7] is widely applied in the literature. It divides the compaction zone into a slip zone, where the roller surface moves faster than the powder bed, and a nip zone, where the powder moves at the same velocity as the rollers. The zones are shown in Fig. 1 together with a porosity profile typically found in ribbons.

Using the Jenike–Shield criterion [35], Johanson postulated expressions for the pressure gradients in both regions. At the nip angle, the two gradients are equal. The main compaction stress develops within the nip region, which is the focus of this work. For a given SCF, the maximum compaction pressure P_{max} can therefore be determined. The required model parameters are summarized in Table 1, along with their measurement methods.

The pressure gradient in the slip zone is defined as:

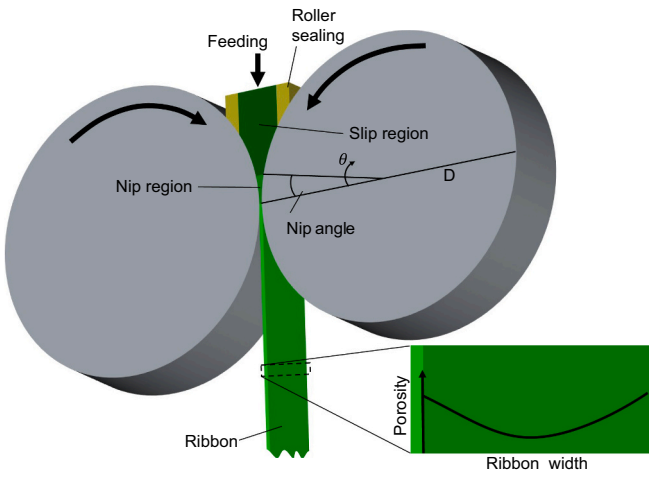

Fig. 1. Drawing of the roller compaction process and Johanson's slip and nip zones. The nip angle separates the slip from the nip region. The setup assumes cheek plates, which are omitted for clarity, along with an exemplary ribbon porosity profile is shown, indicating low porosities in the ribbon center (Note: cheek plates invert the profile).

Table 1
List of model parameters and corresponding measurement methods.

Objective	Parameter	Symbol	Measurement device
Johanson	Effective angle of internal friction	δ_E	Shear cell
	Wall friction angle	ϕ'	Shear cell
	Compressibility factor	K	Tablet press
	Initial porosity	ε_0	Tablet press + caliper
Kawakita	Empirical parameter	a	Tablet press + caliper
	Empirical parameter	b	Tablet press + caliper
Ryshkewitch-Duckworth	Non-porous strength	$\overline{\sigma}$	Tablet analyzer
	Empirical parameter	k	Tablet analyzer
Roller compaction	Roller diameter	D	–
	Roller force	RF	–
	Roller gap	S	–
	Roller width	W	–
	Average pocket thickness	d	–
Tablet press	Tableting pressure	σ	–

$$\left.\frac{d\sigma}{dx}\right|_{Slip} = \frac{4\sigma\left(\frac{\pi}{2}-\theta-\nu\right)\tan(\delta_E)}{\frac{D}{2}\left(1+\frac{S}{D}-\cos(\theta)\right)(\cot(A-\mu)-\cot(A+\mu))}, \tag{1}$$

with

$$A = \frac{\theta}{2}+\frac{\nu}{2}+\frac{\pi}{4}, \tag{2}$$

$$\nu = \frac{\pi}{2}-\arcsin\left(\frac{\sin(\phi')}{\sin(\delta_E)}\right)-\phi', \tag{3}$$

$$\mu = \frac{\pi}{4}-\frac{\delta_E}{2}. \tag{4}$$

Here, σ is the normal stress, D is the roller diameter, θ is the roll angle, S is the roller gap, δ_E is the effective angle of internal friction, and ϕ' is the wall friction angle.

The pressure gradient in the nip zone is given by:

$$\left.\frac{d\sigma}{dx}\right|_{Nip} = \frac{K\sigma_\theta(2\cos(\theta)-1-S/D)\tan(\theta)}{\frac{D}{2}(d/D+(1+S/D-\cos(\theta))\cos(\theta))}, \tag{5}$$

2.3. Kawakita's compressibility model

Compressibility models describe the relationship between compaction pressure and the resulting porosity (or solid fraction). Several models are commonly used, including those of Heckel [18,19], Kawakita [20,21], and Cooper–Eaton [22]. Generally, the accuracy of these models increases with the number of parameters they require: Heckel employs two parameters, Kawakita three, and Cooper–Eaton four. In this study, the Kawakita model is applied because it achieves good predictive accuracy while requiring relatively few fitting parameters, thereby reducing the amount of experimental data needed.

In its linearized form, the Kawakita equation is expressed as:

$$\frac{\sigma}{C} = \frac{1+b\sigma}{ab} \tag{9}$$

where a and b are model parameters, σ is the applied compaction pressure, and C is the relative volume decrease defined as:

$$C = \frac{V_0 - V}{V_0} \tag{10}$$

with V_0 being the initial bulk volume and V the compacted volume.

Rewriting Eq. (9) in terms of porosity yields:

$$\varepsilon = \frac{(1-\varepsilon_0)(1+b\sigma)}{ab\sigma - b\sigma - 1} + 1 \tag{11}$$

where ε is the porosity at compaction pressure σ, and ε_0 is the initial porosity, included as a third model parameter, corresponding to the porosity at zero compaction pressure.

2.4. Compactability model

A widely used method for describing the relationship between tablet tensile strength σ_t and porosity ε was first proposed by Ryshkewitch [36] and later extended by Duckworth [37]:

$$\ln\left(\frac{\sigma_t}{\overline{\sigma}}\right) = -k\varepsilon \tag{12}$$

The model has two input parameters that can be interpreted as pure material tensile strength at zero porosity $\overline{\sigma}$ and empirical parameter k. In practice, both parameters are typically obtained by fitting to experimental data, particularly when different material compositions are investigated.

2.5. Model for tablet porosity

The Johanson model provides the peak stress acting during the RC process. Using Eq. (11), the corresponding ribbon porosity can be estimated, and the porosity difference relative to the initial state can be expressed as:

$$\Delta\varepsilon = \varepsilon_0 - \varepsilon_{ribbon} \tag{13}$$

here ε_0 is the initial porosity of the uncompacted reference material used to fit Eq. (11) (i.e., the starting state of the Kawakita fit), and ε_{ribbon} is the porosity of the compacted ribbon. This porosity difference can be incorporated into Eq. (11) by introducing an additional dimensionless parameter Ψ with exponent $\Delta\varepsilon$:

$$\varepsilon = \left(\frac{(1-\varepsilon_0)(1+b\sigma)}{ab\sigma - b\sigma - 1} + 1\right)\Psi^{\Delta\varepsilon} \tag{14}$$

Ψ is introduced as a lumped interface parameter that maps densification history from roller compaction to effective tablet compressibility, rather than representing new compaction physics. It incorporates machinery impacts (e.g. ribbon porosity profile, milling) and physical effects (e.g. grain hardening, material's elastic recovery and primary

particle/granule size and shape). The advantage of this simple model adjustment is that it preserves the uncompacted material properties, since for $\Delta\varepsilon = 0$, Eq. (14) reduces to the original Kawakita relationship.

2.6. Model for strength of tablets of dry granules

Analogous to the estimation of tablet porosity, an additional empirical parameter Ω in the unit of pressure is introduced to account for granule hardening due to pre-compaction, as well as machinery setup. It therefore depends on the ribbon's porosity profile, milling conditions and elastic recovery. Incorporating the porosity difference $\Delta\varepsilon$, the Ryshkewitch–Duckworth relationship (Eq. (12)) can be extended as:

$$\sigma_t = \sigma_{RyD}\left(\frac{\sigma_{RyD}}{\Omega}\right)^{\Delta\varepsilon} \tag{15}$$

This model extension applies both to dry-granulated granules and to direct compaction. In the special case $\Delta\varepsilon = 0$, Eq. (15) reduces to the original Ryshkewitch–Duckworth formulation Eq. (12).

2.7. Modeling pipeline

The proposed model for estimating final tablet porosity and tensile strength relies on the parameters listed in Table 1. These are divided into material-specific parameters, which can be determined from standard laboratory experiments, and machine parameters. For cases where only small amounts of powder are available, micro shear cells can be used to determine the (wall) yield locus, e.g., FT4 (Freeman Technology Ltd., ~1 mL), RST (Dr. Dietmar Schulze GmbH, <10 mL), or MCR Evolution (Anton Paar GmbH, <5 mL).

The first step is the determination of material-dependent parameters. With these parameters, the nip angle is calculated using the Johanson model, which provides the maximum compaction pressure P_{max} via Eq. (7). The value of P_{max} can be used as the compaction pressure σ in the Kawakita model Eq. (11), allowing the ribbon porosity to be derived. Ribbon and granule porosity are assumed to be equal. From this, $\Delta\varepsilon$ can be determined and the tablet porosity can be predicted via Eq. (14), provided that Ψ is known or calibrated.

In the next step, the tablet tensile strength can be estimated using Eq. (15) with the calibrated Ω either by applying the experimental tablet porosity or the model-predicted porosity from Eq. (14). The full pipeline is presented in Fig. 2, including the calibration routes.

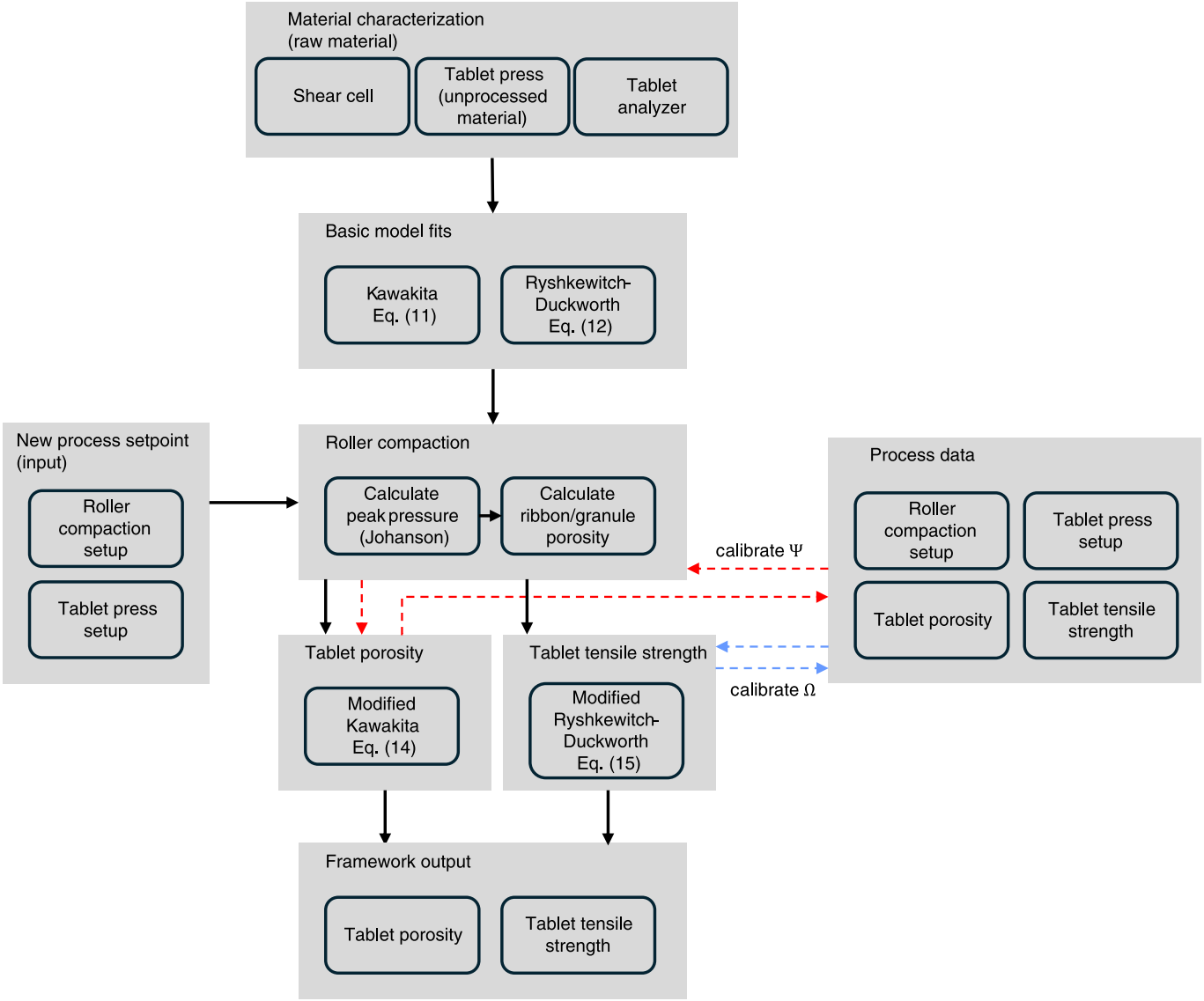

Fig. 2. Schematic of the reduced-order modeling framework linking roller compaction to tablet properties and tensile strengths.

3. Results

3.1. Sensitivity analysis

A variance-based sensitivity analysis of all parameters in Table 1 was performed to quantify their influence on the model outputs (tablet porosity and tensile strength). The Sobol' method [38–41], including second-order interactions, was applied. The resulting total effect indices (S_T) are summarized in Table 2 for both outputs (tablet porosity and tensile strength). The Sobol' total effect index S_T quantifies the overall contribution of an input parameter to the variance of the model output, including its main effect and all interaction effects with other parameters. Values close to zero indicate negligible influence, whereas larger values indicate increasing importance. Parameter boundaries used in the analysis are also given.

Sampling was performed according to the Saltelli scheme [39] with a base sample size of 3000, resulting in 78,000 model runs (12 parameters) for porosity and 90,000 model runs (14 parameters) for tensile strength. Parameters not included in the respective output model were not sampled and are therefore marked as "-" in Table 2.

For tablet porosity, the most influential parameters were the tableting pressure (σ) and the Kawakita parameters ε_0 and a. For tensile strength, all parameters except those specific to the Johanson model showed strong influence. The roller diameter (D) shows a relatively large confidence interval, most likely due to the wide range defined by its parameter boundaries.

3.2. Model evaluation

Rajkumar et al. [27] investigated tablets produced from RC granules of microcrystalline cellulose (MCC) and mannitol at different porosities. Data for the Johanson model were also reported in their study. The material parameters for the Johanson, Kawakita and Ryshkewitch-Duckworth models (Table 1) were either fitted to data or taken directly from Rajkumar et al. [27]. All fits within this paper were performed using the Levenberg-Marquardt algorithm of SciPy [42].

In the following sections, the prediction of tablet porosity is discussed (Section 3.2.1) and compared against experimental data. This is followed by the prediction of tablet tensile strength by using experimentally determined tablet porosity (Section 3.2.2) and finally, in Section 3.2.3, the predicted porosity is used for the prediction of the tensile strength and response surface maps are derived.

3.2.1. Tablet porosity

The calculation steps for the present model are as follows. First, the empirical parameters of the Kawakita model (Eq. (11)) – namely a, b, and ε_0 – were fitted to experimental data obtained from non-precompacted powder. In the second step, the ribbon (or granule) porosity was estimated as a function of the SCF. For this purpose, the maximum pressure predicted by the Johanson model was calculated, and the corresponding ribbon porosity was derived using the fitted Kawakita model. Finally, the empirical parameter Ψ was determined by fitting Eq. (14) to the experimental data of Rajkumar et al. [27].

For MCC, Ψ was fitted to 0.65, resulting in an $R^2 = 0.99$. Applying the same Ψ value to mannitol yielded an $R^2 = 0.96$, demonstrating the applicability of the parameter. Although a different Ψ could improve the fit for mannitol, a constant value of 0.65 was retained for both materials for the sake of simplicity. The corresponding model predictions are shown in Fig. 3.

Table 2
Total sensitivity indices (S_T) with 95% confidence intervals (CI) for porosity and tensile strength, along the boundaries used in the sensitivity analysis. * indicates that tableting pressure (σ) was sampled logarithmically.

		Porosity	Tensile strength	Boundaries	
Symbol	Unit	$S_T \pm CI$	$S_T \pm CI$	Min	Max
δ_E	°	0.169 ± 0.030	0.072 ± 0.030	0.1	80
ϕ'	°	0.108 ± 0.029	0.057 ± 0.069	0.01	50
K	–	0.011 ± 0.005	0.002 ± 0.001	0.5	20
ε_0	–	0.350 ± 0.044	0.242 ± 0.055	0.3	0.7
a	–	0.323 ± 0.033	0.586 ± 0.172	10^{-6}	0.8
b	1/MPa	0.042 ± 0.009	0.063 ± 0.019	10^{-6}	1
$\bar{\sigma}$	MPa	–	0.401 ± 0.164	1	30
k	–	–	0.093 ± 0.022	1	30
D	m	0.024 ± 0.009	0.120 ± 0.208	0.01	0.5
S	m	0.014 ± 0.009	0.001 ± 0.001	$5{\cdot}10^{-4}$	0.01
d	m	0.024 ± 0.009	0.001 ± 0.001	0	$5{\cdot}10^{-3}$
σ	Pa	0.566 ± 0.067	0.520 ± 0.111	10^4 *	$5{\cdot}10^8$ *
Ψ	–	0.181 ± 0.034	–	0	10
Ω	MPa	–	0.171 ± 0.070	0.5	100
SCF	kN/cm	0.022 ± 0.009	0.003 ± 0.002	0.5	40

3.2.2. Tablet tensile strength

The Ryshkewitch–Duckworth parameters $\bar{\sigma}$ and k were determined by fitting Eq. (12) to experimental data. Using the ribbon porosity calculated in the previous section, the additional empirical parameter Ω was then fitted via Eq. (15) to the MCC data. It should be noted that the experimental tablet porosities were available and directly used for the fitting procedure.

For MCC, $\Omega = 16.0$ MPa resulted in a coefficient of determination of $R^2 = 0.98$. Applying the same Ω value to mannitol yielded an excellent fit as well, with $R^2 = 0.99$. Although an alternative value of could slightly improve the fit for mannitol, the same parameter was retained for both materials to maintain simplicity. The corresponding model predictions are shown in Fig. 4.

3.2.3. Combined model

In contrast to the previous section, where tablet tensile strength was estimated using experimentally determined porosity values, tensile strength can also be predicted by applying the porosity calculated in Section 3.2.1. Due to error propagation, the predictive performance is reduced, yielding $R^2 = 0.83$ for MCC and $R^2 = 0.81$ for mannitol.

Model response surface plots for tablet porosity and tensile strength are presented in Figs. 5 and 6. With respect to porosity (Fig. 5), increasing SCF and tableting pressure both lead to a decrease in tablet porosity. For the plastically deforming MCC, the effect of SCF levels off at 10 kN/cm, while the more brittle mannitol exhibits a stronger and more persistent response to SCF. For MCC, the influence of SCF becomes negligible above 10 kN/cm because MCC deforms predominantly plastically and undergoes pronounced granule hardening during roller compaction. Once a certain densification level is reached, additional SCF causes only minor further changes in the granule's ability to deform during tableting, so tablet porosity and tensile strength are then mainly governed by the tableting pressure. This loss of tabletability by dry

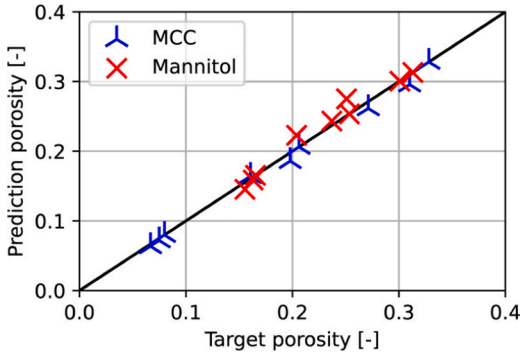

Fig. 3. Parity plot comparing model-predicted tablet porosity (y-axis) with experimentally measured tablet porosity (x-axis) for MCC and mannitol. Each marker represents one experimental condition; agreement with the diagonal y = x indicates accurate prediction.

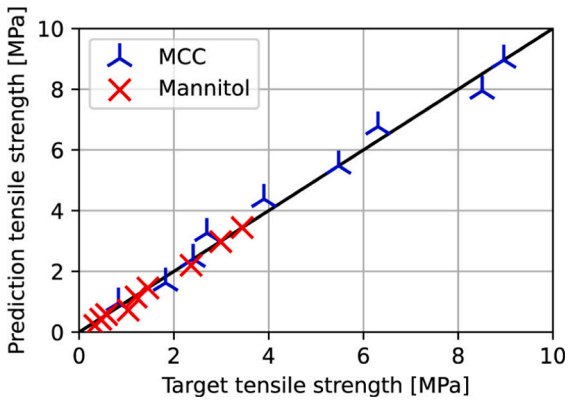

Fig. 4. Parity plot comparing model-predicted tablet tensile strength (y-axis) with experimentally measured tensile strength (x-axis) for MCC and mannitol. Each marker corresponds to one experimental condition. Proximity to the diagonal y = x indicates predictive accuracy.

granulation is a well-known effect for plastically deforming excipients such as MCC [26]. In contrast, mannitol is more brittle and its tableting behavior is dominated by fragmentation, so that an increase in SCF further alters granule/fine particle formation and bonding conditions during tableting, resulting in a more sustained SCF effect across the range studied [27]. Moreover, MCC tablets show a broader porosity range compared to mannitol.

Regarding tensile strength (Fig. 6), similar trends are observed. Increasing SCF results in decreasing tensile strength, with diminished influence above 10 kN/cm for MCC but remaining pronounced for mannitol. Overall, MCC tablets exhibit higher tensile strength than mannitol tablets at the compared processing conditions.

Finally, the empirical parameters Ψ and Ω can be fitted simultaneously to the experimental data for each material. Using the averaged goodness of fit, defined as

$$\overline{R^2} = \frac{R^2_{Porosity} + R^2_{Strength}}{2} \tag{16}$$

the overall predictive performance was improved, resulting in $\overline{R^2} = 0.94$ for MCC and $\overline{R^2} = 0.96$ for mannitol.

3.3. Assumptions and limitations

The simplicity of the proposed framework is achieved at the expense of several assumptions, which entail the following limitations. First, the applied Johanson model assumes a one-dimensional pressure distribution along the roller circumference, and therefore neglects any variation across the roller width. Consequently, lateral (axial) variations in ribbon porosity cannot be captured. Moreover, the Johanson model does not account for roll-speed or dwell-time effects. For ductile materials such as MCC, higher roll speeds may increase ribbon porosity due to reduced dwell time and altered deformation behavior of the primary particles [43]. These effects are not explicitly considered in the present

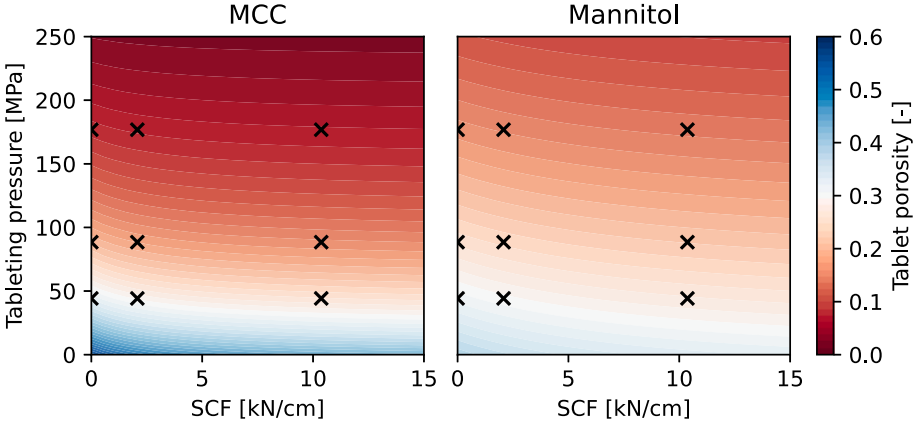

Fig. 5. Framework contour plot of tablet porosity as a function of SCF and tableting pressure for MCC and mannitol. Color levels indicate constant tablet porosity, showing that increasing SCF and/or tableting pressure reduces porosity. Cross markers denote the experimental conditions from [27].

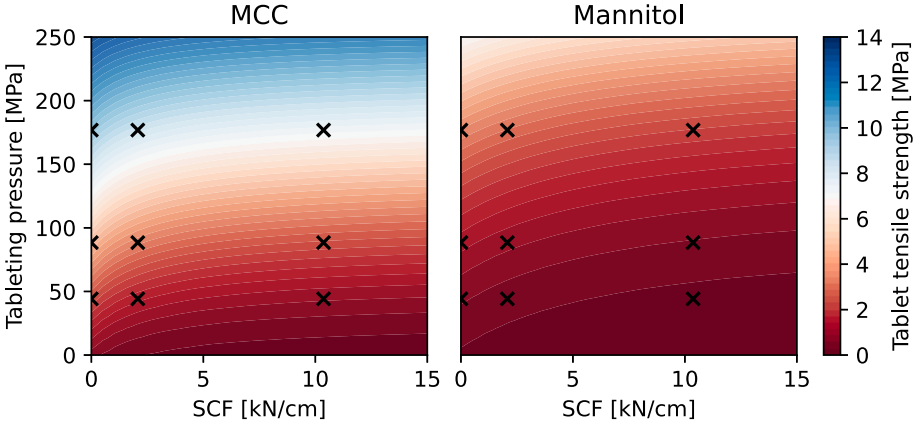

Fig. 6. Framework contour plot of tablet tensile strength as a function of SCF and tableting pressure for MCC and mannitol. Color levels indicate constant tensile strength. Increasing tableting pressure increases tensile strength, whereas increasing SCF generally decreases tensile strength. Cross markers denote the experimental conditions from [27].

framework.

Second, elastic recovery of the ribbon after compaction is not accounted for. This simplification is considered acceptable within the scope of the model, since the framework targets a reduced-order description rather than a detailed physical representation, and porosity heterogeneity within the ribbon is neglected anyway.

Third, the subsequent milling step is not explicitly modeled. Depending on the equipment manufacturer, different milling mechanisms are employed, most commonly integrated screening mills that allow only particles below a defined size to pass. In the proposed framework, milling is neglected for the sake of simplicity. As a result, the granule size distribution is not considered, although it is often bimodal, consisting of granules and residual primary particles, and strongly depends on the ribbon porosity [44,45]. In addition, granules can exhibit porosities that differ from the parent ribbon: depending on their origin within the ribbon and their breakage mechanism, porosity may even increase due to micro-cracking. Nevertheless, because ribbon porosity is assumed homogeneous, using the ribbon porosity as a surrogate for granule porosity is a reasonable first-order approximation within the present framework.

Finally, in the subsequent tableting step, tablet press settings, tablet geometry, and granule properties can substantially influence tablet porosity and tensile strength. These variations cannot be resolved explicitly by the framework and are therefore lumped into the interface parameters Ψ and Ω. Hence, Ψ and Ω should be regarded as process- and equipment-specific calibration constants and will change if the process configuration (roller compactor, mill, or tablet press) is modified.

4. Discussion and conclusion

The presented approach supports two main use cases. First, it enables parameter exploration for new material compositions, allowing estimation of the required RC settings to achieve the desired tablet properties. Second, when experimental data from tablets produced with RC granules are available, a more precise model can be derived by fitting the empirical parameters Ψ and Ω, for example, in a model-based design of experiments. However, the simplicity of the model, relying on only one empirical factor each for porosity and tensile strength, also introduces certain limitations. The ribbon and granule porosity derived from the Johanson and Kawakita models should be regarded as artificial measures and not as the true physical porosity. Since ribbons exhibit a porosity distribution across their width, representing them with a single value is an oversimplification. Similarly, the model does not account for granule size, which in reality may influence tablet strength by modifying the available bonding surface. Nonetheless, such simplifications are common; for example, other implementations [28] also neglect particle size effects. In the reduced-order framework, unresolved ribbon porosity heterogeneity and granule effects are represented in lumped form by the interface parameters Ψ and Ω.

In addition to roller compaction and internal milling, of course tablet press conditions also affect final tablet properties. Even when restricting the analysis to cylindrical tablets, dwell time is known to play an important role, particularly for plastically deforming materials, by reducing elastic recovery and increasing strength [43]. These influences are likewise captured indirectly by the empirical parameters. Importantly, both Ω and Ψ depend not only on the material but also on the specific machinery used. The fact that their values remain similar across MCC and mannitol suggests that machine effects may outweigh material-specific effects, which must be considered when comparing data obtained on different equipment.

Despite these limitations, the framework demonstrates significant advantages in terms of simplicity. It provides a unified framework for viewing the dry granulation route as a single, continuous process rather than a set of isolated unit operations. Furthermore, alternative models for predicting ribbon porosity or for describing tablet tensile strength and porosity could be substituted into this framework and can be linked through $\Delta\varepsilon$ and the lumped parameters Ψ and Ω.

Finally, the framework can be extended to incorporate dissolution behavior, as demonstrated by Gavi et al. [28], offering further opportunities for integrated process modeling.

The proposed framework is not intended to replace established formulation-development tools (e.g. compaction simulations). Instead, it provides an alternative process scale-up and transferring settings between devices when historical data for the equipment are available.

CRediT authorship contribution statement

Christian Eichler: Writing – original draft, Visualization, Conceptualization. **Stefan Heinrich:** Writing – review & editing, Supervision.

Funding sources

This research did not receive any specific grant from funding agencies in the public, commercial, or not-for-profit sectors.

Declaration of competing interest

The authors declare that they have no known competing financial interests or personal relationships that could have appeared to influence the work reported in this paper.

Data availability

Data will be made available on request.

References

[1] R. Wiedey, P. Kleinebudde, The density distribution in ribbons from roll compaction, in: Chem. Ing. Tech. 89, 2017, pp. 1017–1024, https://doi.org/10.1002/cite.201600143.
[2] C.S. Omar, R.B. Al-Asady, A.D. Salman, Roller compaction: improving the homogeneity of ribbon properties along the roller width, Powder Technol. 342 (2019) 464–474, https://doi.org/10.1016/j.powtec.2018.10.018.
[3] C. Eichler, S. Pietsch-Braune, M. Dosta, A. Schmidt, S. Heinrich, Micromechanical analysis of roller compaction process with DEM, Powder Technol. 398 (2022) 117146, https://doi.org/10.1016/j.powtec.2022.117146.
[4] O. Simon, P. Guigon, Interaction between feeding and compaction during lactose compaction in a laboratory roll press, KONA 18 (2000) 131–138, https://doi.org/10.14356/kona.2000019.
[5] A.M. Miguélez-Morán, C.-Y. Wu, H. Dong, J.P.K. Seville, Characterisation of density distributions in roller-compacted ribbons using micro-indentation and X-ray micro-computed tomography, Eur. J. Pharm. Biopharm. 72 (2009) 173–182, https://doi.org/10.1016/j.ejpb.2008.12.005.
[6] A. Michrafy, H. Diarra, J.A. Dodds, M. Michrafy, Experimental and numerical analyses of homogeneity over strip width in roll compaction, Powder Technol. 206 (2011) 154–160, https://doi.org/10.1016/j.powtec.2010.04.030.
[7] J.R. Johanson, A rolling theory for granular solids, J. Appl. Mech. 32 (1965) 842–848, https://doi.org/10.1115/1.3627325.
[8] G. Bindhumadhavan, J.P.K. Seville, M.J. Adams, R.W. Greenwood, S. Fitzpatrick, Roll compaction of a pharmaceutical excipient: experimental validation of rolling theory for granular solids, Chem. Eng. Sci. 60 (2005) 3891–3897, https://doi.org/10.1016/j.ces.2005.02.022.
[9] A. Michrafy, H. Diarra, J.A. Dodds, M. Michrafy, L. Penazzi, Analysis of strain stress state in roller compaction process, Powder Technol. 208 (2011) 417–422, https://doi.org/10.1016/j.powtec.2010.08.037.
[10] J.C. Cunningham, Experimental Studies and Modeling of the Roller Compaction of Pharmaceutical Powders, Doctoral dissertation, Drexel University, Philadelphia, Pennsylvania, United States, 2005.
[11] M. Bi, F. Alvarez-Nunez, F. Alvarez, Evaluating and modifying Johanson's rolling model to improve its predictability, J. Pharm. Sci. 103 (2014) 2062–2071, https://doi.org/10.1002/jps.24012.
[12] R. Sousa, P.C. Valente, M. Nakach, L. Bardet, M. Wacquet, N. Midoux, J.-R. Authelin, Roller compaction scale-up made simple: an approximate analytical solution to Johanson's rolling theory, J. Pharm. Sci. 109 (2020) 2536–2543, https://doi.org/10.1016/j.xphs.2020.05.004.
[13] G. Reynolds, R. Ingale, R. Roberts, S. Kothari, B. Gururajan, Practical application of roller compaction process modeling, Comput. Chem. Eng. 34 (2010) 1049–1057, https://doi.org/10.1016/j.compchemeng.2010.03.004.
[14] V.V. Nesarikar, C. Patel, W. Early, N. Vatsaraj, O. Sprockel, R. Jerzweski, Roller compaction process development and scale up using Johanson model calibrated with instrumented roll data, Int. J. Pharm. 436 (2012) 486–507, https://doi.org/10.1016/j.ijpharm.2012.06.027.

[15] A.V. Zinchuk, M.P. Mullarney, B.C. Hancock, Simulation of roller compaction using a laboratory scale compaction simulator, Int. J. Pharm. 269 (2004) 403–415, https://doi.org/10.1016/j.ijpharm.2003.09.034.
[16] H.L. Reimer, P. Kleinebudde, Hybrid modeling of roll compaction processes with the Styl'One evolution, Powder Technol. 341 (2019) 66–74, https://doi.org/10.1016/j.powtec.2018.02.052.
[17] L. Beccaro, P. Facco, R.M. Dhenge, M.J. Khala, F. Cenci, F. Bezzo, M. Barolo, Accelerating pharmaceutical tablet development by transfer of powder compaction equipment across types and scales, Int. J. Pharm. 667 (2024) 124904, https://doi.org/10.1016/j.ijpharm.2024.124904.
[18] R.W. Heckel, An analysis of powder compaction phenomena, Trans. Metall. Soc. AIME 221 (1961) 1001–1008.
[19] R.W. Heckel, Density-pressure relationships in powder compaction, Trans. Metall. Soc. AIME 221 (1961) 671–675.
[20] K. Kawakita, Y. Tsutsumi, A comparison of equations for powder compression, Bull. Chem. Soc. Jpn. 39 (1966) 1364–1368, https://doi.org/10.1246/bcsj.39.1364.
[21] K. Kawakita, K.-H. Lüdde, Some considerations on powder compression equations, Powder Technol. 4 (1971) 61–68, https://doi.org/10.1016/0032-5910(71)80001-3.
[22] A.R. Cooper, L.E. Eaton, Compaction behavior of several ceramic powders, J. Am. Ceram. Soc. 45 (1962) 97–101, https://doi.org/10.1111/j.1151-2916.1962.tb11092.x.
[23] H.L. Keizer, P. Kleinebudde, Elastic recovery in roll compaction simulation, Int. J. Pharm. 573 (2020) 118810, https://doi.org/10.1016/j.ijpharm.2019.118810.
[24] K. Vorländer, L. Bahlmann, A. Kwade, J.H. Finke, I. Kampen, Influence of compression kinetics during tableting of fluidized bed-granulated microorganisms on microbiological and physical-mechanical tablet properties, Eur. J. Pharm. Biopharm. 188 (2023) 161–169, https://doi.org/10.1016/j.ejpb.2023.05.012.
[25] A.A. Ouazzou, Y.M. Harshe, V. Meunier, J.H. Finke, S. Heinrich, Influence of process parameters and particle size distribution on mechanical properties of tablets, Chemie Ingenieur Technik 95 (2023) 168–177, https://doi.org/10.1002/cite.202200157.
[26] C.C. Sun, P. Kleinebudde, Mini review: mechanisms to the loss of tabletability by dry granulation, Eur. J. Pharm. Biopharm. 106 (2016) 9–14, https://doi.org/10.1016/j.ejpb.2016.04.003.
[27] A.D. Rajkumar, G.K. Reynolds, D. Wilson, S.A.C. Wren, A.D. Salman, The effect of roller compaction and tableting stresses on pharmaceutical tablet performance, Powder Technol. 341 (2019) 23–37, https://doi.org/10.1016/j.powtec.2018.08.065.
[28] E. Gavi, G.K. Reynolds, System model of a tablet manufacturing process, Comput. Chem. Eng. 71 (2014) 130–140, https://doi.org/10.1016/j.compchemeng.2014.07.026.
[29] L. Farber, K.P. Hapgood, J.N. Michaels, X.-Y. Fu, R. Meyer, M.-A. Johnson, F. Li, Unified compaction curve model for tensile strength of tablets made by roller compaction and direct compression, Int. J. Pharm. 346 (2008) 17–24, https://doi.org/10.1016/j.ijpharm.2007.06.022.
[30] L.R. White, M. Molloy, R.J. Shaw, G.K. Reynolds, System model driven selection of robust tablet manufacturing processes based on drug loading and formulation physical attributes, Eur. J. Pharm. Sci. 172 (2022) 106140, https://doi.org/10.1016/j.ejps.2022.106140.
[31] S. Bachawala, R.B. Lagare, A.B. Delaney, Z.K. Nagy, G.V. Reklaitis, M. Gonzalez, Rational function-based approach for integrating tableting reduced-order models with upstream unit operations: dry granulation case study, Pharmaceuticals 17 (2024) 1158, https://doi.org/10.3390/ph17091158.
[32] N. Boersen, M.T. Carvajal, K.R. Morris, G.E. Peck, R. Pinal, The influence of API concentration on the roller compaction process: modeling and prediction of the post compacted ribbon, granule and tablet properties using multivariate data analysis, Drug Dev. Ind. Pharm. 41 (2015) 1470–1478, https://doi.org/10.3109/03639045.2014.958754.
[33] L. Mareczek, C. Riehl, M. Harms, S. Reichl, Analysis of the impact of material properties on tabletability by principal component analysis and partial least squares regression, Eur. J. Pharm. Sci. 200 (2024) 106836, https://doi.org/10.1016/j.ejps.2024.106836.
[34] L. Mareczek, C. Riehl, M. Harms, S. Reichl, Elucidating the impact of material properties on tablet manufacturability for binary paracetamol blends, Pharm. Res. 41 (2024) 185–197, https://doi.org/10.1007/s11095-023-03626-6.
[35] A.W. Jenike, R.T. Shield, On the plastic flow of coulomb solids beyond original failure, J. Appl. Mech. 26 (1959) 599–602, https://doi.org/10.1115/1.4012119.
[36] E. Ryshkewitch, Compression strength of porous sintered alumina and zirconia: 9th communication to ceramography, J. Am. Ceram. Soc. 36 (1953) 65–68, https://doi.org/10.1111/j.1151-2916.1953.tb12837.x.
[37] W. Duckworth, Discussion of Ryshkewitch paper by Winston Duckworth*, J. Am. Ceram. Soc. 36 (1953) 68, https://doi.org/10.1111/j.1151-2916.1953.tb12838.x.
[38] I.M. Sobol', Global sensitivity indices for nonlinear mathematical models and their Monte Carlo estimates, Math. Comput. Simul. 55 (2001) 271–280, https://doi.org/10.1016/S0378-4754(00)00270-6.
[39] A. Saltelli, P. Annoni, I. Azzini, F. Campolongo, M. Ratto, S. Tarantola, Variance based sensitivity analysis of model output. Design and estimator for the total sensitivity index, Comput. Phys. Commun. 181 (2010) 259–270, https://doi.org/10.1016/j.cpc.2009.09.018.
[40] T. Iwanaga, W. Usher, J. Herman, Toward SALib 2.0: advancing the accessibility and interpretability of global sensitivity analyses, SESMO 4 (2022) 18155, https://doi.org/10.18174/sesmo.18155.
[41] J. Herman, W. Usher, SALib: an open-source Python library for sensitivity analysis, JOSS 2 (2017) 97, https://doi.org/10.21105/joss.00097.
[42] P. Virtanen, R. Gommers, T.E. Oliphant, M. Haberland, T. Reddy, D. Cournapeau, E. Burovski, P. Peterson, W. Weckesser, J. Bright, et al., SciPy 1.0: fundamental algorithms for scientific computing in Python, Nat. Methods 17 (2020) 261–272, https://doi.org/10.1038/s41592-019-0686-2.
[43] S. Berkenkemper, Mechanical Deformation Behavior of Materials during Compression, Doctoral dissertation, Heinrich-Heine-Universität Düsseldorf, Düsseldorf, Germany, 2023.